Sādhanā (2019) 44:35
https://doi.org/10.1007/s12046-018-1027-3

Three-dimensional flow separations on a rolling sphere

PRAVIN K VEREKAR and JAYWANT H ARAKERI*

Department of Mechanical Engineering, Indian Institute of Science, Bangalore 560012, India
e-mail: jaywant@mecheng.iisc.ernet.in

MS received 22 December 2017; revised 3 July 2018; accepted 6 September 2018; published online 25 January 2019

Abstract. Experiments are conducted to study the flow separations on a sphere rolling on an inclined plane submerged in water. These experiments are performed at Reynolds numbers *Re* between 1350 and 1550. The experiments show that the flow separations on the surface of a rolling sphere can be organized into four distinct regions: (i) region of primary separation-I on the front upper sphere and extending below the poles, (ii) region of viscous blockage at the crevice surrounding the point of contact and shear layer separation ahead and at the sides of the viscous blockage, (iii) region of primary separation-II on the rear lower sphere and (iv) secondary separations on the rear upper sphere surface. The ratio of the width of the viscous blockage to the diameter of the sphere is found to be 0.4. Primary separation-I surface is symmetrical about the equatorial plane of the rolling sphere. Primary separation-II from the rear lower sphere surface is asymmetrical about the equator and eddies are shed alternately on either side of the equator from this separation surface. These lower eddies are energetic and dominate the dynamics of the wake. The upper eddy shedding from the primary separation-I surface and the lower eddy shedding from the primary separation-II surface are synchronized.

Keyword. Boundary layer separation; vortex shedding; wake; rolling sphere.

1. Introduction

Flow separations on the surface of a rolling sphere are investigated using flow visualization techniques. Near-wake behind the rolling sphere is studied using Particle Image Velocimetry (PIV) experiments in addition to flow visualization methods. Knowing the flow separations and their subsequent evolution into distinct flow structures is a step towards understanding the fluid forces acting on the sphere and the dynamics of the rolling sphere.

Flow separations for cylinders and spheres have been studied extensively in the literature. The classical problem of flow past an isolated stationary cylinder has been reviewed by Williamson [1]. The wake behind the cylinder is steady, consisting of two symmetrical standing eddies for Reynolds numbers *Re* up to 49. When *Re* is near 49, the steady wake becomes unstable to small disturbances; the instability first appears in the wake at some distance behind the cylinder, giving rise to oscillation of the wake. As *Re* is increased, the wake oscillations affect the standing eddies and at a critical value of the Reynolds number (depending on experimental conditions) eddies are shed on each side of the cylinder alternately; this wake comprising two rows of staggered eddies of opposite rotation sense is known by the name Kármán vortex street.

Flow past a rotating cylinder has been studied for *Re* up to 200. Recent studies include Akoury *et al* [2] and Stojković *et al* [3]. Apart from the Reynolds number *Re*, the flow is also governed by another parameter, the dimensionless rotation rate $\alpha = D\omega/2U_0$ where D is the cylinder diameter, ω the constant angular velocity of the cylinder rotation and U_0 the free-stream velocity. As α is increased, at a certain value the eddy shedding stops and the wake disappears. Stewart and co-workers [4–6] have conducted studies on flow past a rolling cylinder. Wake characteristics depend on *Re* and α.

Constantinescu and Squires [7] have comprehensively reviewed the work on flow past an isolated stationary sphere. For flows with Reynolds number *Re* below 20, the entire flow region is laminar and there is no separation. For *Re* between 20 and 400 a stationary vortex ring is formed behind the sphere; this vortex ring begins to oscillate around *Re* of 400. Between Reynolds numbers 400 and 800, there is laminar hairpin-like large-scale vortex shedding behind the sphere. The shedding is a result of the spiral instability seen as a progressive wave motion with alternate fluctuations generated by the shear present at the boundary between the recirculation region and the outside flow, the Strouhal number (*St*) for the same being roughly constant at 0.18–0.2. At a threshold Reynolds number of 800 and beyond, the periphery of the recirculation zone is prone to Kelvin–Helmholtz instability and the separated shear layer breaks into small vortex tubes. At higher Reynolds

*For correspondence

numbers, the Strouhal numbers associated with the Kelvin–Helmholtz instability increase due to shear layers becoming unstable to smaller wavelengths. The large-scale structures in the subcritical regime eventually become turbulent while retaining their hairpin-shaped form. Beyond the critical point $Re = 380,000$ in the supercritical regime, the shedding of large-scale hairpin vortices is at higher frequency ($St \approx 1.3$) and the wake is narrower. These large-scale structures are shed periodically and regularly into the wake but become difficult to visualize experimentally because of the absence of spiral instability. One can see that there are differences in the characteristic length- and time scales associated with shedding of large-scale vortices as one moves from subcritical flows to supercritical flows.

The problem of laminar flow about a rotating sphere in a fluid at rest has been solved analytically by Howarth [8]. The presence of centrifugal forces causes a secondary flow in the boundary layer whereby the fluid particles move along the surface of the sphere spiralling away from the poles towards the equator. There is flow into the boundary layer near the poles, and out of it at the equator. A transversely rotating sphere in free-stream exhibits Magnus effect, and this phenomenon is put to good use by sports persons in games like tennis, cricket, football, etc. Aerodynamics of sports balls is explained by Mehta [9, 10] and Asai *et al* [11]. Giacobello *et al* [12] have numerically studied flow past a transversely rotating sphere at Reynolds numbers *Re* of 100, 250 and 300.

The problem of a non-rotating sphere that is touching a plane and moving parallel to it with constant velocity in an ideal fluid at rest is studied analytically by Cox and Cooker [13]. They show that the flow velocities are high near the point of contact and the velocity becomes infinite at the point of contact. Stewart *et al* [14, 15], Bolnot [16] and Rao *et al* [17] have studied flow past a rolling sphere. Their studies are for Reynolds numbers between 75 and 350. Rao *et al* [17] have identified two successive transitions; the first transition from steady to unsteady wake, but the wake remaining strictly periodic, occurs at $Re \approx 139$ and, the second transition, which involves a loss of planar symmetry and a low-frequency lateral oscillation of the wake, occurs at $Re \approx 192$. In these studies [14–17], the rolling sphere is constrained to prevent its lateral displacement.

Our experiments are performed using a solid rigid smooth sphere rolling down an inclined plane submerged in quiescent water. These experiments are performed at Reynolds numbers *Re* between 1350 and 1550. The motivation for these experiments comes from a need to generate new research information on flow separations of a class of solid–fluid interaction problems that involve rolling sphere geometry. This information can be applied to problems such as sediment transport, movement of gravel on the ocean floor and the river bed due to water currents, in sports having sphere rolling on the ground, etc.

2. Description of experiments

Experiments are performed in a glass tank 61 cm long by 15 cm wide by 14 cm deep. The rectangular tank, at one of its end, has levelling screws on either side. The levelling screws allow the tank to be tilted to a desired angle.

The tank is filled with water and the sphere is released from rest on the false bottom plane of the tank. The sphere rolls down the plane under the influence of gravity; its initial motion is with decreasing acceleration until it attains terminal velocity. An acrylic solid sphere of diameter $D = 2.54$ cm and density $\rho = 1180\ \mathrm{kg/m^3}$ is used. The sphere is transparent. For our experiments, its surface is coloured black. The inclination angles of the tank for the experiments are chosen between 3° and 4°. Verekar and Arakeri [18] report on the kinematics of the rolling motion of the sphere used in these experiments. The terminal velocities are found to be between 5.5 and 6.0 cm/s. The terminal velocities are attained at S/D approximately equal to 4.5 where S is the distance travelled by the sphere on the inclined plane from the point of release. The Reynolds numbers *Re* are based on the diameter of the sphere and its terminal velocity.

Flow visualization experiments are performed using tracer particles and fluorescein dye. When fluorescein dye is used for the experiments, the dye is either introduced on the surface of the sphere as a thin layer using a pipette and then the sphere is allowed to roll down, or the dye is laid as a thin layer on the entire inclined plane and then the sphere is released to roll down. Experiments demanding planar visualization are performed with laser light sheet illumination. Whole-flow-field visualizations are performed using incandescent lamps for the lighting and a Canon PowerShot A480 camera for the photography.

For the flow visualization experiments using tracer particles, the water in the tank is seeded with silver-coated hollow glass spheres of 14 μm diameter. These glass spheres are manufactured by Potters Industries Inc., and their product name is CONDUCT-O-FIL and designation SH400S33. These tracer particles have been previously used by experimenters for seeding water flows and they have been found to follow the local flow velocity faithfully. In our experiments, the tracer particles are illuminated by a light sheet about 2-mm thick, formed by passing a laser beam through a plano-concave lens of focal length 10 mm. Argon-ion continuous laser Stabilite 2017, manufactured by Spectra-Physics Lasers operating at 488.0 nm with maximum power output of 1.5 W, is used as the light source. A Photron FASTCAM-PCI R2 model 500 digital camera is used for the photography.

PIV experiments are also performed to study the near-wake. PIV experiments yield quantitative data of the velocity field, the vorticity, the flow structures in the wake, and the spatial and the temporal evolution of these entities. The same tracer particles described earlier are used in these

PIV experiments. The maximum flow velocity in our experiments is within 10 cm/s. For such low speed flow, the digital image pair for PIV analysis can be acquired at a time delay Δt in milliseconds. Also, low-speed flow allows flexibility in choosing image exposure time; the exposure time is important in order to avoid tracer particles appearing as streaks in the digital image. We have conducted PIV experiments using an Argon-ion continuous laser and Photron digital camera. PIV method is discussed in detail in Raffel *et al* [19]. The PIV data in our case are acquired after the sphere has rolled a distance S beyond $4.5D$, where the sphere attains terminal velocity U_0. The PIV measurement results are presented with the flow velocity vector $\vec{u}$ normalized by the terminal velocity U_0 of the sphere and the vorticity ω as a dimensionless number $\omega D/U_0$.

The laser light sheets for the planar visualizations are taken in three different orientations: (i) vertical longitudinal XZ planes parallel to the lengthwise sides of the water tank, (ii) XY planes parallel to the inclined plane and at different heights from it and (iii) the vertical transverse or the cross-sectional YZ planes. The XZ plane is shown in figure 1. The origin of the XYZ Cartesian coordinate system is fixed at the point of contact of the sphere and the inclined plane. Since the point of contact is instantaneously at rest (see Ziegler [21]), our frame of reference is fixed to the water tank. All our observations and measurements are made in this absolute frame of reference. Our experimental observations are in top view by looking in the $-Z$ direction, in rear end view by looking in the $-X$ direction and in side view by looking in $+Y$ or $-Y$ direction.

3. Experimental observations and discussion

When the sphere starts rolling down the inclined plane, it produces an irrotational flow field in the surrounding water. The streamlines of the irrotational flow begin on the front surface of the sphere and end on the rear surface. The presence of the inclined plane (also called tangent plane) bisects the rearward moving flow below the lower hemisphere near the point of contact; Cox and Cooker [13] have shown that the flow velocities are comparatively very high here. The viscous effects are felt in the water that is in contact with the sphere surface. This viscous shear layer adjacent to the sphere surface, which is a region of vorticity, grows in thickness with lapse of time, and the vorticity is then swept behind the sphere as a wake by the induced irrotational flow. The irrotational flow produced behind the sphere now stands modified by the presence of the wake. Hence, the flow field surrounding the rolling sphere moving with terminal velocity U_0 consists of (i) a large region of water, ahead of and to the side of the sphere, in which the flow is approximately irrotational, (ii) a thin viscous shear layer adjacent to the surface and (iii) the wake containing detached vorticity.

The photographs in figure 2 show the wake behind the sphere, which is rolling down the inclined plane from left to right. The fluorescein dye had been introduced on the surface of the sphere before setting it rolling. The sphere is at a distance $S/D = 8.0$ in the top photograph and at $S/D = 9.0$ in the bottom photograph. A noteworthy feature of the wake is its zigzag appearance; this is unlike the wake behind an isolated sphere translating in a fluid. Wake of the isolated sphere remains confined around the axis that passes through the centre of the sphere and is aligned with the

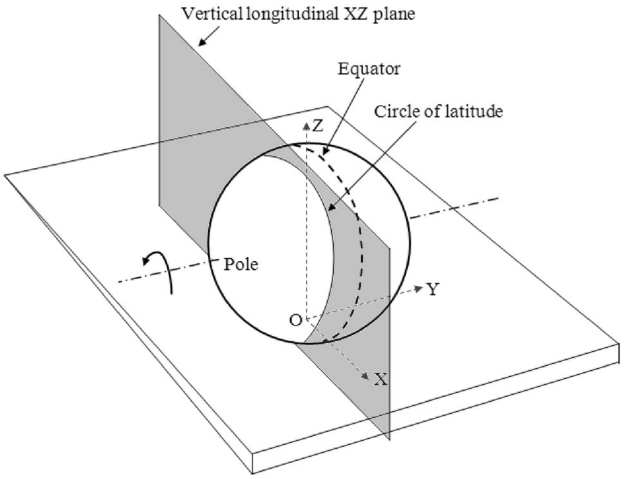

Figure 1. Configuration for the rolling sphere is shown. Origin O is the point of contact between the rolling sphere and the inclined plane.

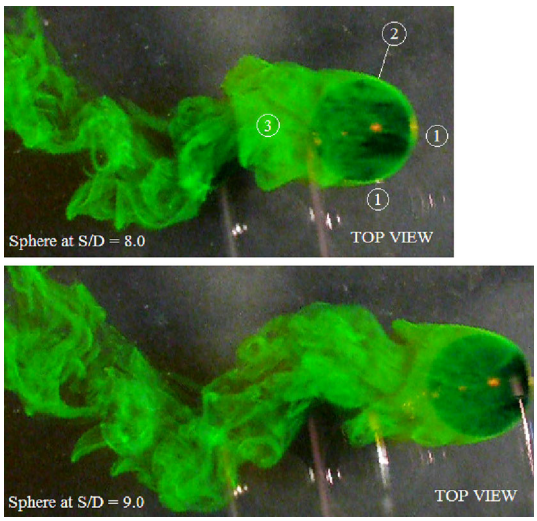

Figure 2. As the sphere rolls on the inclined plane, its wake, which is made visible by the dye, is seen in top view in the photographs. The sphere rolls from left to right. An incandescent lamp is used for lighting. The reflected image of the camera in the inclined glass plane is partly seen in the photographs. Experimental conditions are Reynolds number $Re \approx 1500$ and sphere velocity $U_0 \approx 6$ cm/s. Legend: (1) region of irrotational flow ahead and around the sphere, (2) boundary layer and (3) wake. TOP PHOTOGRAPH: The sphere is at a distance $S/D = 8.0$. BOTTOM PHOTOGRAPH: It is at a distance $S/D = 9.0$.

sphere velocity vector. In the movie of this experiment, it is seen that the near-wake sways alternately on either side of the equatorial plane $Y = 0$ and its formation is periodic in time and space. We define non-dimensional time $t^\star$ as tU_0/D where t is the time beginning from a reference start point. The near-wake sways alternately about the equatorial plane with time period $(\Delta t^\star)_{period} = 2.0$ and spatial period $(\Delta S)_{period} = 2.0D$. The alternating lateral orientations of the wake suggest the presence of alternately directed side-forces on the rolling sphere. The side-force effects are seen in our experiments; a sphere that is released from rest on the inclined plane often deviates from the path of being parallel to the sides of the water tank. For the PIV experiments, the travel path of the rolling sphere should remain aligned in the laser light sheet plane. To prevent deviation of the trajectory, the sphere motion on the inclined plane is guided by a rail about 5.5-mm wide made from 0.25-mm-diameter brass wires. The rails are laid centrally on the inclined plane.

By an assiduous study of the flow visualizations and the PIV results obtained from our experiments, we discern remarkable organization in the features of the flow separations occurring on the rolling sphere surface. The flow separations seen on the surface of the rolling sphere can be organized into four distinct regions: (i) region of primary separation-I on the front upper sphere and it extends below the poles, (ii) separation on the front and sides of the viscous blockage at the crevice surrounding the point of contact, (iii) region of primary separation-II on the rear lower sphere surface above the crevice region and (iv) secondary separations on the rear upper sphere surface. These four regions are explained in sections 3.1–3.4 and they are shown in figure 3.

3.1 *Region of primary separation-I*

The photograph in figure 4 is taken from the movie of the experiment performed with fluorescein dye laid on the sphere. In the photograph, the white curve marks the line of flow separation. This line of flow separation is clearly discernible in the movie. This separation line is termed as primary separation-I line. The dashed part of the white curve is the hidden line, since this part of the curve lies on the sphere surface below the separated layer. The dashed line ends at the spiral node of separation. The spiral node of separation is explained in Patel [20]. The existence of the spiral node of separation is clearly realized from the photograph in figure 16. The primary separation-I line runs on the sphere on either side of the equator because the flow separation from this line is symmetrical about the equatorial plane (see figures 5–7 and 16). Another observation that can be made from the movie is that there is a separate trail of eddies from the lower rear sphere surface. This will be discussed in section 3.3.

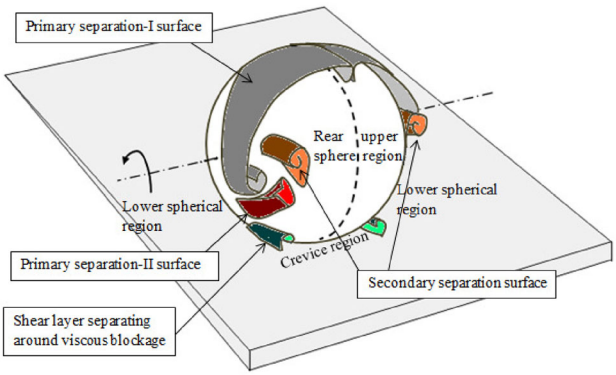

Figure 3. Sketch showing the flow separations on the surface of the rolling sphere.

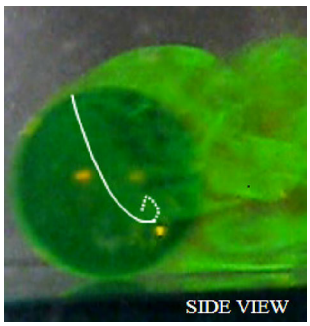

Figure 4. The sphere rolls from right to left in the photograph. Fluorescein dye is laid on the sphere. The white curve shown on the sphere surface demarcates the primary separation-I line. $Re \approx 1500$ and $U_0 \approx 6$ cm/s.

In figure 5, the tracer particles in the water are illuminated by laser light sheet at $Z = 5D/6$. In the photographs, the sphere rolls from right to left and it has moved a distance of one diameter from its position in figure 5a to its position in figure 5c. The stationary tracer particles are seen as white dots, while the particles in the wake flow are seen as white streaks. The white curve in the photographs is drawn to indicate the trace of the separated surface, which is more clearly seen in the movie of the experiment; the dashed part of the white curve is drawn for continuity in the shadow of the sphere. A trace is a curve formed by the intersection of a plane and a curved surface. The symmetry of the separated primary separation-I surface is clearly visible. This symmetry can also be seen in the vertical transverse plane $X = D/2$ shown in figure 16. From figure 5b, it is observed that the eddies are shed on either side of the equator simultaneously. In the photographs in figure 5a and c, the rolling sphere is in the midst of the same phase of the eddy shedding cycle from the primary separation-I surface. We conclude that one cycle of eddy shedding is completed in one diameter displacement of the sphere.

The PIV results of the near-wake on the planes $Z = 5D/6$ and $Z = D/2$ (see figures 6 and 7) confirm that eddies shed from the primary separation-I surface are

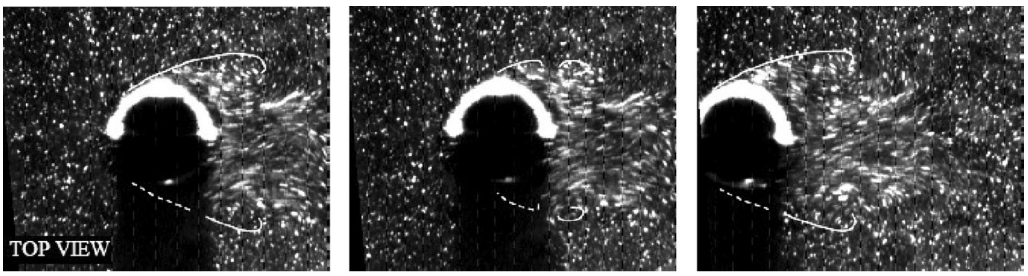

Figure 5. Photographs show the trace (highlighted in white curve) of the separated surface from primary separation-I line as viewed in the laser light sheet at $Z = 5D/6$. The laser light sheet shines from top to bottom in the photographs. The sphere rolls from right to left and has moved a distance $1.0D$ from its position in figure (**a**) to its position in figure (**c**). Eddies are shed in figure (**b**). $Re \approx 1500$ and $U_0 \approx$ 6 cm/s.

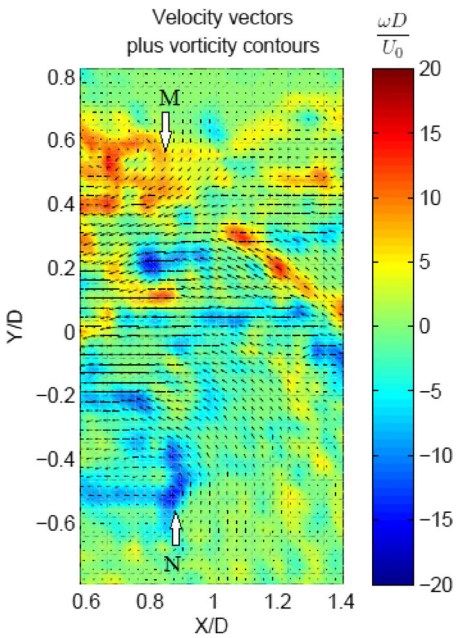

Figure 6. The eddies M and N resulting from primary separation-I as seen on plane $Z = 5D/6$ in the PIV results.

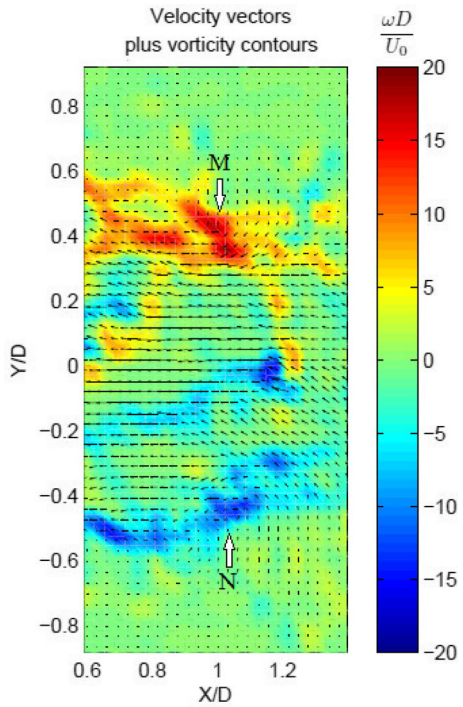

Figure 7. The eddies M and N resulting from primary separation-I as seen on plane $Z = D/2$ in the PIV results.

symmetrical about the equatorial plane $Y = 0$. Clockwise eddy (i.e., red colour eddy) resulting from the separated surface on one side of the equatorial plane is marked by letter M and anticlockwise eddy (i.e., blue colour eddy) on the other side of the plane is marked by N. Symmetry of eddies M and N is easily noticeable. Subsequent PIV measurements show that these eddies detach at the same time.

3.2 *Crevice region*

The space between the inclined plane and the sphere, surrounding the point of contact, is called the crevice. Experiments are conducted wherein fluorescein dye is laid as a thin layer on the inclined plane and the sphere is then allowed to roll down. Snapshots of the movie of such an experiment are shown in figure 8. It can be seen that the rolling sphere sets aside the dye around the point of contact, leaving a trail of clear water. The width of the trail close to the sphere is measured to be equal to $0.4D$. The setting aside of the dye behind the point of contact can be explained as follows. The rolling sphere is instantaneously stationary at the point of contact (see Ziegler [21]). Water in the crevice surrounding the point of contact is in contact with the nearly stationary sphere surface at the top and with the stationary inclined plane surface at the bottom. The no-slip boundary condition at the top and bottom of the crevice region ensures the volume of water in the crevice to be instantaneously stationary. This stationary water at the crevice region obstructs the irrotational flow occurring

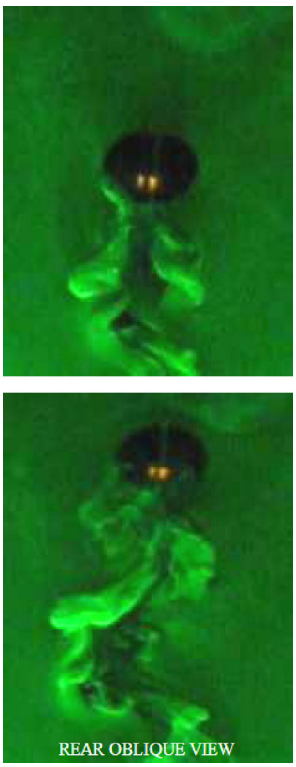

Figure 8. Rear oblique view of the sphere rolling down the inclined plane on which a thin layer of fluorescein dye is laid. $Re \approx 1500$ and $U_0 \approx 6$ cm/s.

below the lower hemisphere. The velocity field for the irrotational flow over the inclined plane is shown in figure 9 (see Verekar [23]). We call the stationary water, which blocks this flow, as viscous blockage. A schematic diagram of the viscous blockage is shown in top view in figure 10a and in rear view in figure 10b.

The photograph in figure 11 is taken from the experiment where fluorescein dye is introduced on the sphere. In the photograph, the vertical transverse laser light sheet at $X = 0.75D$ illuminates the dye in the near-wake from the left. Symmetrical eddies close to the inclined plane, which are marked by arrows in the photograph, are seen; the eddy on the left is rotating clockwise and the one on the right is rotating anticlockwise. The reflection of these eddies in the inclined glass plane is seen towards the bottom of the photograph. These eddies originate from the sides of the viscous blockage at the crevice. It appears to us that a horse-shoe vortex has formed ahead and on the sides of the viscous blockage. Fackrell and Harvey [22] have found similar eddies, in front and on the sides of a rolling wheel, close to the ground plane.

3.3 *Primary separation-II from rear lower sphere surface*

The photographs in figure 12 show the wake as seen in the laser light sheet at $Z = D/6$. The sphere is moving from left

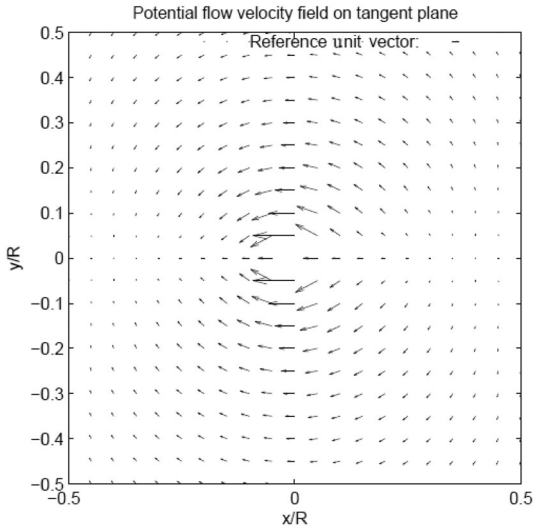

Figure 9. Figure shows velocity field for the potential flow on the tangent plane around the point of contact in absolute frame of reference. The sphere of unit radius translates from left to right with unit velocity; the point of contact is at the origin. R is the radius of the sphere.

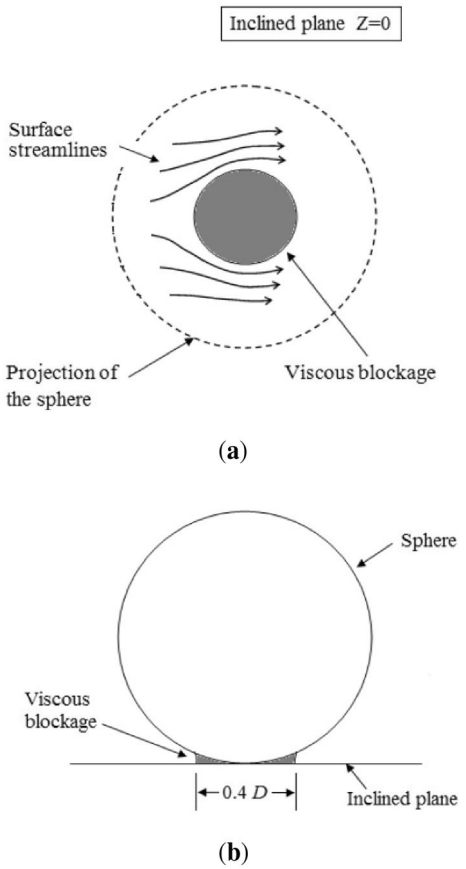

Figure 10. Schematic showing streamlines around the viscous blockage and close to the tangent plane in top view in (**a**) and schematic of the viscous blockage in rear view in (**b**). In (**a**), sphere rolls from right to left.

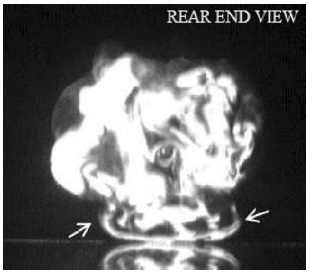

Figure 11. The wake is seen in the laser light sheet at $X = 0.75D$. Fluorescein dye is released on the sphere and the laser light sheet from the left illuminates it. Arrows indicate eddies originating from either side of the viscous blockage. Towards the bottom of the photograph, part of the reflection in the inclined glass plane is seen. $Re \approx 1500$ and $U_0 \approx$ 6 cm/s.

to right in the photographs, and it is at a distance $S/D = 7.0$ in figure 12a and is at $S/D = 8.0$ in figure 12b. In figure 12a, eddy A is shed and eddy B is getting formed. The eddy B detaches in figure 12b after the sphere has moved a distance $1.0D$ and eddy C is getting formed on the other side of the equatorial plane $Y = 0$. These lower eddies A–C are shed alternately on either side of the equator. The spatial period of one cycle of this lower eddy shedding (from eddy A to eddy C) occurs in a sphere motion of $2.0D$.

Flow visualization experiments conducted using tracer particles illuminated in the vertical transverse laser light sheet give further understanding of these lower eddies. Two snapshots from the movies of these experiments are shown in figure 13. In figure 13a, a representative of the evolving eddy B (anticlockwise rotation) of the earlier figure 12a is

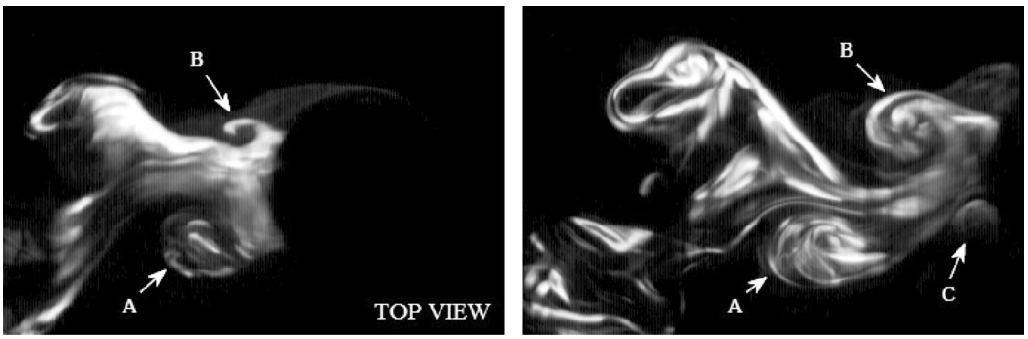

(**a**) (**b**)

Figure 12. The wake is seen in top view in the laser light sheet at $Z = D/6$. Fluorescein dye is introduced on the sphere. The laser light sheet shines from top to bottom in the photographs. The sphere rolls from left to right. It is at $S/D = 7.0$ in (**a**) and is at $S/D = 8.0$ in (**b**). Outline of the sphere can be noted in the photographs. $Re \approx 1500$ and $U_0 \approx$ 6 cm/s.

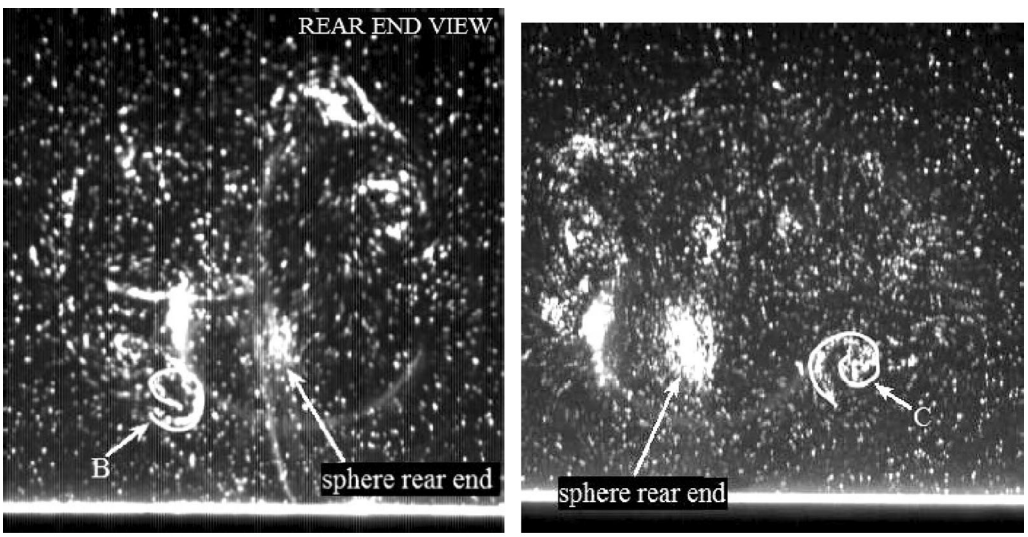

(**a**) (**b**)

Figure 13. Tracer particles are illuminated by the laser light sheet at $X = D/2$. The sphere rolls through the plane of the paper away from the reader. The sphere rear end is seen illuminated by the laser light. The horizontal white thick line illumination near the bottom of the photographs is of tracer particles deposited on the surface of the inclined glass plane. White curve demarcates left-side lower eddy B in (**a**) and right-side lower eddy C in (**b**). These eddies B and C are the same ones mentioned in figure 12. $Re \approx 1500$ and $U_0 \approx$ 6 cm/s.

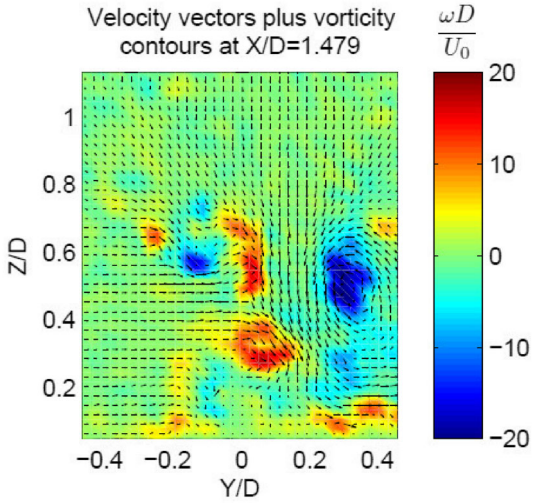

Figure 14. PIV results of the wake in the plane $X = 1.5D$.

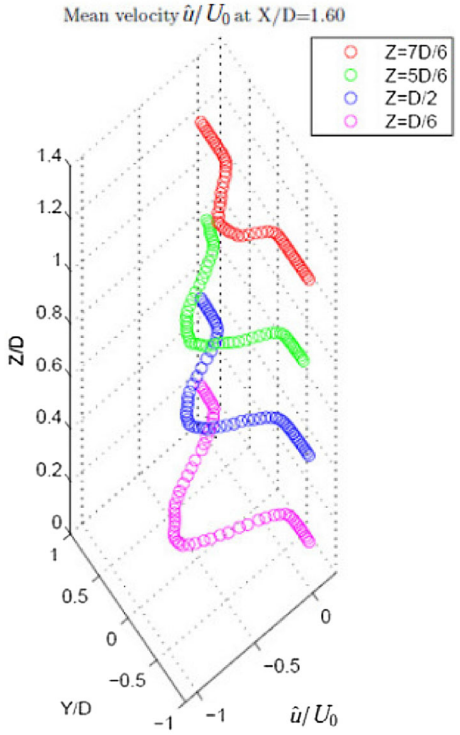

Figure 15. Ensemble average velocity $\hat{u}$ of the wake on the planes $Z = D/6$, $Z = D/2$, $Z = 5D/6$ and $Z = 7D/6$ at the station $X/D = 1.6$.

seen in the plane $X = D/2$, while in figure 13b, which is taken from another experiment, representative of the evolving eddy C (clockwise rotation) of the earlier figure 12b is seen in the plane $X = D/2$. Close examination of the movies of our flow visualization experiments shows that these alternately shed lower eddies translate upwards and shift laterally towards the equatorial plane and progressively move across this plane, and they are responsible for the zigzag shape of the wake seen in figure 2.

PIV results of the wake in the vertical transverse plane $X = 1.5D$ taken from one of the experiments are shown in figure 14. In the figure, the blue-colour anticlockwise eddy is the representative of the eddy B in figure 13a. The eddy B, seen here in the plane $X = 1.5D$, has moved across the equatorial plane $Y = 0$. As seen from the PIV measurements, the lower eddies are energetic; they are tornado-like vortices and they dominate the dynamics of the wake. The separation curve on the lower rear sphere surface from which the lower eddies have evolved is named as the primary separation-II line. This is shown in figure 3.

3.4 *Region of secondary separations behind the rear upper sphere*

The flow in the wake is unsteady and has forward velocities (see figure 15). We have calculated ensemble average velocity $\hat{u}(X, Y)$ on different XY planes at different stations $X = const.$ from a collection of experiments. The ensemble average $\hat{u}$ is calculated on planes $Z = D/6$, $Z = D/2$, $Z = 5D/6$ and $Z = 7D/6$ from 1156, 1337, 788 and 1124 velocity fields, respectively. Figure 15 shows a plot of the normalized average velocity $\hat{u}/U_0$ on different XY planes at the station $X/D = 1.6$.

Flow-separated surfaces behind the upper sphere are visible in the experiments conducted using vertical transverse laser light sheet. In figure 16, tracer particles are illuminated at $X = D/2$. White curves are drawn on the photograph to demarcate traces of the primary separation-I surface (P1–Q1 and P2–Q2) and traces of the secondary separation surfaces (R1, R2). It can be seen from figure 16 that the secondary separation surfaces disturb the primary separation-I surface and folds are developed on the primary separation-I surface. The formation of the secondary separation is explained as follows.

The flow velocities are high in the central region behind the rolling sphere in the vicinity of the equatorial plane. This is seen from the PIV measurements of the velocity field on the plane $Z = D/2$ shown in figure 17. This high-velocity flow, which can reach a maximum magnitude of nearly $1.5U_0$, impinges on the rear central equatorial region of the rolling sphere translating with velocity U_0. On this rear surface, which is moving upwards, this flow is symmetrically deflected outwards away from the equatorial plane. The equatorial plane is the dividing surface for this flow. The deflected flow moves obliquely on the rear upper sphere surface until it separates and forms eddies. These separations, here on the rear upper surface, are termed as secondary separations and the eddies are termed as secondary eddies. The secondary eddies R1 and R2 lie below the primary separation-I surface.

Figure 18 gives velocity field of the wake in the plane $Y = D/3$ at a particular instant. Verekar [23] gives

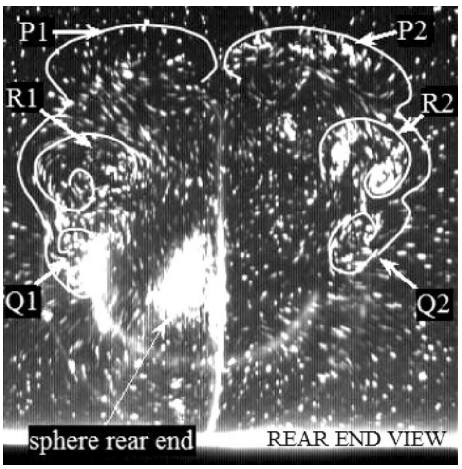

Figure 16. Tracer particles are illuminated by the laser light sheet at $X = D/2$. The sphere rear end is also illuminated by the laser light. White curves demarcate the traces of the primary separation-I surface (P1-Q1 and P2-Q2) and those of the secondary separation surfaces (R1, R2). $Re \approx 1500$ and $U_0 \approx$ 6 cm/s.

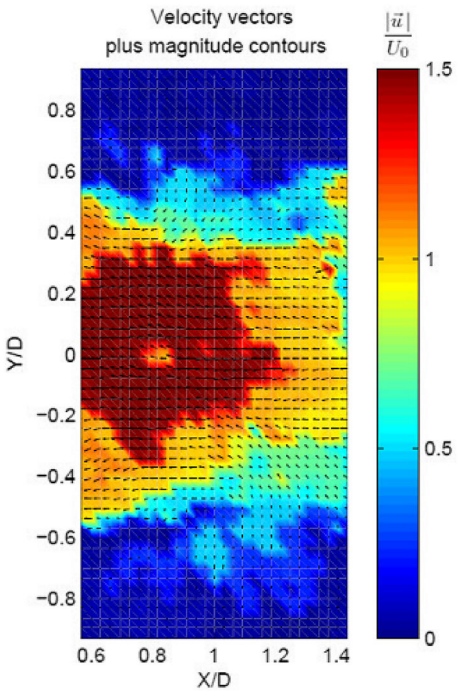

Figure 17. PIV results of the wake in the plane $Z = D/2$.

detailed analyses of the PIV data of the problem discussed in this paper.

It is now opportune to discuss the eddy shedding cycle. In figure 16, it is seen that the primary separation-I surface and the secondary separation surfaces are symmetrical about the equatorial plane. However, this symmetry is lost when the one-sided lower eddy from the primary separation-II surface gets detached as seen in figure 13. Figure 13 presents the phase of the eddy shedding cycle when the

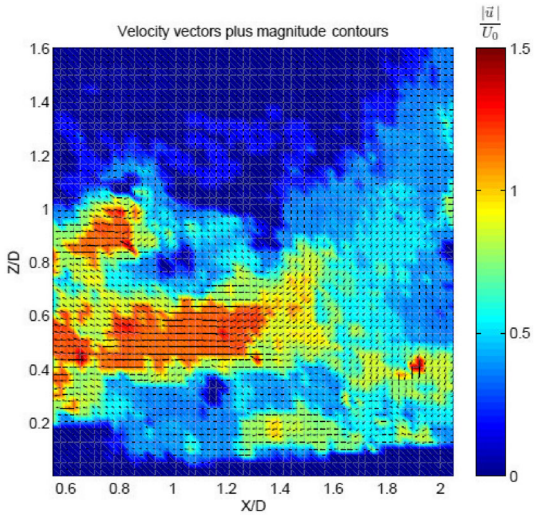

Figure 18. PIV results of the wake in the plane $Y = D/3$.

eddies are shed, and the lower eddy shed from the primary separation-II surface obliterates the flow symmetry that existed about the equatorial plane because of the symmetry of the primary separation-I surface and the secondary separation surfaces. Verekar [23] has shown that the upper and the lower eddy sheddings are synchronized; by this it is meant that these eddies are shed simultaneously.

4. Conclusions

Figure 3 shows a sketch of the flow separations on the surface of the rolling sphere, consistent with our experimental observations and discussion. At the crevice region, surrounding the point of contact of the sphere and the inclined plane, is the viscous blockage, which is a near-stationary volume of water. A horse-shoe vortex is formed ahead and at the sides of the viscous blockage. Primary separation-I line runs symmetrically on either side of the equator on the sphere from the upper front surface to right down below the poles as shown. Primary separation-II line is on the lower rear sphere surface and flow separations occur alternately on either side of the equator from this separation line. Eddy sheddings from separation-I and separation-II are synchronized. Secondary flow separations, which are symmetrical, are formed on the upper rear surface in tandem with primary flow separation-I. The eddies detaching from primary separation-II are tornado-like and are responsible for the zigzag shape of the wake.

References

[1] Williamson C H K 1996 Vortex dynamics in the cylinder wake. *Annu. Rev. Fluid Mech.* 28: 477–539

[2] Akoury R, Braza M, Perrin R, Harran G and Hoarau Y 2008 The three-dimensional transition in the flow around a rotating cylinder. *J. Fluid Mech.* 607: 1–11

[3] Stojković D, Schön P, Breuer M and Durst F 2003 On the new vortex shedding mode past a rotating circular cylinder. *Phys. Fluids* 15(5): 1257–1260

[4] Stewart B E, Hourigan K, Thompson M C and Leweke T 2006 Flow dynamics and forces associated with a cylinder rolling along a wall. *Phys. Fluids* 18(11): 111701

[5] Stewart B E, Thompson M C, Leweke T and Hourigan K 2010 The wake behind a cylinder rolling on a wall at varying rotation rates. *J. Fluid Mech.* 648: 225–256

[6] Rao A, Stewart B E, Thompson M C, Leweke T and Hourigan K 2011 Flows past rotating cylinders next to a wall. *J. Fluids Struct.* 27: 668–679

[7] Constantinescu G and Squires K 2004 Numerical investigations of flow over a sphere in the subcritical and supercritical regimes. *Phys. Fluids* 16: 1449–1466

[8] Howarth L 1951 Note on the boundary layer on a rotating sphere. *Philos. Mag. VII* 42: 1308–1315

[9] Mehta R D 1985 Aerodynamics of sports balls. *Annu. Rev. Fluid Mech.* 17: 151–189

[10] Mehta R D 2005 An overview of cricket ball swing. *Sports Eng.* 8: 181–192

[11] Asai T, Seo K, Kobayashi O and Sakashita R 2007 Fundamental aerodynamics of the soccer ball. *Sports Eng.* 10: 101–109

[12] Giacobello M, Ooi A and Balachandar S 2009 Wake structure of a transversely rotating sphere at moderate Reynolds numbers. *J. Fluid Mech.* 621: 103–130

[13] Cox S J and Cooker M J 2000 Potential flow past a sphere touching a tangent plane. *J. Eng. Math.* 38: 355–370

[14] Stewart B E, Leweke T, Hourigan K and Thompson M C 2008 Wake formation behind a rolling sphere. *Phys. Fluids* 20(7): 071704

[15] Stewart B E, Thompson M C, Leweke T and Hourigan K 2010 Numerical and experimental studies of the rolling sphere wake. *J. Fluid Mech.* 643: 137–162

[16] Bolnot H, Passaggia P Y, Leweke T and Hourigan K 2011 Wake transition of a rolling sphere. *J. Visual.* 14(1): 1–2

[17] Rao A, Passaggia P Y, Bolnot H, Thompson M C, Leweke T and Hourigan K 2012 Transition to chaos in the wake of a rolling sphere. *J. Fluid Mech.* 695: 135–148

[18] Verekar P K and Arakeri J H 2010 Sphere rolling down an incline submerged in a liquid. In: Prasad B V S S S (ed.) *Proceedings of the Thirty-Seventh National and Fourth International Conference on Fluid Mechanics and Fluid Power*, IIT Madras, Valardocs, Chennai

[19] Raffel M, Willert C E, Wereley S T and Kompenhans J 2007 *Particle image velocimetry*. Springer, Berlin

[20] Patel V C 1993 Three-dimensional flow separation. *Sadhana* 18: 553–574

[21] Ziegler H 1965 *Mechanics*, vol. II. Addison-Wesley, Boston

[22] Fackrell J E and Harvey J K 1973 The flow field and pressure distribution of an isolated road wheel. In: Stephens H S (ed.) *Advances in Road Vehicle Aerodynamics*. BHRA Fluid Engineering, Cranfield, Bedford, England

[23] Verekar P K 2012 *Experiments on rolling sphere submerged in an incompressible fluid*. Ph.D. Thesis, Indian Institute of Science, Bangalore